

Friction-enhanced lifetime of bundled quantum vortices

Luca Galantucci

*Istituto per le Applicazioni del Calcolo 'M. Picone',
IAC-CNR, Via dei Taurini 19, 00185 Roma, Italy and
Joint Quantum Centre (JQC) Durham–Newcastle,
and School of Mathematics and Statistics, Newcastle University,
Newcastle upon Tyne, NE1 7RU, United Kingdom*

Giorgio Krstulovic

*Université Côte d'Azur, Observatoire de la Côte d'Azur, CNRS, Laboratoire Lagrange,
Boulevard de l'Observatoire CS 34229 - F 06304 NICE Cedex 4, France*

Carlo F. Barenghi

*Joint Quantum Centre (JQC) Durham–Newcastle,
and School of Mathematics and Statistics, Newcastle University,
Newcastle upon Tyne, NE1 7RU, United Kingdom.*

(Dated: March 8, 2023)

We show that a toroidal bundle of quantized vortex rings in superfluid helium generates a large-scale wake in the normal fluid which reduces the overall friction experienced by the bundle, thus greatly enhancing its lifetime, as observed in experiments. This collective effect is similar to the drag reduction observed in systems of active, hydrodynamically cooperative agents such as bacteria in aqueous suspensions, fungal spores in the atmosphere and cyclists in pelotons.

I. INTRODUCTION

Some physical systems consist of components which interact with each others not only directly but also indirectly by changing the common background, leading to remarkable collective effects such as drag reduction. Examples are aqueous suspensions of self-propelled bacteria¹⁻³, fungal spores⁴, road racing cyclists in the peloton^{5,6}, and particles trapped inside an optical vortex^{7,8}. Here we report a similar collective effect for quantized vortex rings, fundamental nonlinear excitations of superfluid helium. Vortex rings are generated in the laboratory by injecting electrons⁹⁻¹¹, forcing liquid helium through orifices¹² or moving a grid¹³. At sufficiently low temperatures, a single, isolated superfluid vortex ring of radius R is an Hamiltonian object¹⁴ traveling at constant energy ($\propto R$) and velocity ($\propto 1/R$). At higher temperatures, liquid helium has a two-fluid nature: thermal excitations (phonons and rotons) form a viscous gas called the normal fluid which interacts with quantized vortices via a mutual friction force. Because of this friction, a superfluid vortex ring moving in a quiescent normal fluid loses energy, shrinks, speeds up and vanishes.

Here we show that the dynamics of a sufficiently compact toroidal bundle of *many* vortex rings is remarkably different: besides interacting directly with each others in a peculiar leapfrogging fashion, the vortex rings also interplay indirectly by modifying the common normal fluid background. This reduces drastically the total friction so that the bundle remains coherent as if the normal fluid were almost absent, resulting in an enhanced lifetime. Such unusual long life of superfluid vortex bundles has been observed in experiments¹⁵⁻¹⁷, but never explained until now.

In experiments¹⁵⁻¹⁷, large-scale vortex ring structures identified as vortex bundles were generated by forcing liquid helium out of a cylindrical tube. Position and translational velocity of the structures were measured acoustically, together with the spatial distributions of superfluid and normal fluid circulations. It was found that, over a wide temperature range ($1.3 < T < 2.15$ K, corresponding to the superfluid fraction changing from 96% to 0.13%) the bundles remained relatively compact, conserving their initial shape and moving at constant speed over distances of the order of 7 times their initial diameter. The measured superfluid and normal fluid circulations were both of the order of $10^3\kappa$, where κ is the quantum of circulation of one single ring. This fact suggests that such fluid structures consisted of a bundle of $\approx 10^3$ superfluid vortex rings embedded in a normal fluid vortex structure of the same circulation, traveling together across the apparatus.

II. MODEL AND NUMERICAL EXPERIMENT

Our model builds on the Vortex Filament (VF) theory of Schwarz¹⁸, a widely used approach^{19,20} which describes vortex lines as space curves $\mathbf{s}(\xi, t)$ of infinitesimal thickness moving according to

$$\dot{\mathbf{s}}(\xi, t) = \frac{\partial \mathbf{s}}{\partial t} = \mathbf{v}_s + \alpha \mathbf{s}' \times \mathbf{v}_{ns} - \alpha' \mathbf{s}' \times (\mathbf{s}' \times \mathbf{v}_{ns}), \quad (1)$$

where $\mathbf{s}' = \partial \mathbf{s} / \partial \xi$, $\mathbf{v}_{ns} = \mathbf{v}_n - \mathbf{v}_s$ at \mathbf{s} , α and α' are temperature-dependent friction coefficients²¹, \mathbf{v}_n is the normal fluid velocity at \mathbf{s} , and \mathbf{v}_s is the superfluid velocity induced at \mathbf{s} by the entire vortex configuration \mathcal{L} via

$$\mathbf{v}_s(\mathbf{s}, t) = \frac{\kappa}{4\pi} \oint_{\mathcal{L}} \frac{\mathbf{s}'_1(\xi_1, t) \times (\mathbf{s} - \mathbf{s}_1(\xi_1, t))}{|\mathbf{s} - \mathbf{s}_1(\xi_1, t)|^3} d\xi_1. \quad (2)$$

The original VF model consists of Eqs. (1) - (2) and an algorithm to perform vortex reconnections. Its limitation is that the normal fluid velocity \mathbf{v}_n is imposed *a priori*, neglecting the back-reaction of the superfluid vortex lines on \mathbf{v}_n . Recent experiments^{22,23} suggest that normal fluid wakes may form behind each individual vortex line. To account for this effect, which is crucial to understand quantized vortex bundles, we couple Eqs. (1) and (2) self-consistently with the Navier-Stokes equations for \mathbf{v}_n supplemented with a mutual friction force \mathbf{F}_{ns} :

$$\frac{\partial \mathbf{v}_n}{\partial t} + (\mathbf{v}_n \cdot \nabla) \mathbf{v}_n = -\frac{1}{\rho} \nabla p_n + \nu_n \nabla^2 \mathbf{v}_n + \frac{\mathbf{F}_{ns}}{\rho_n} \quad (3)$$

$$\mathbf{F}_{ns} = \oint_{\mathcal{L}} \mathbf{f}_{ns}(\mathbf{s}) \delta(\mathbf{x} - \mathbf{s}) d\xi, \quad \nabla \cdot \mathbf{v}_n = 0. \quad (4)$$

Here \mathbf{f}_{ns} is the local friction per unit length, $\rho = \rho_n + \rho_s$ is the total density of liquid helium, ρ_n and ρ_s are respectively the normal fluid and superfluid densities, p_n is the effective pressure, and ν_n the kinematic viscosity of the normal fluid. We refer to Eqs. (1) - (4) as the coupled Navier-Stokes Vortex Filament (NS-VF) model²⁴. Further details and comparisons with previous approaches²⁵⁻²⁸ are in described in Appendices B and C.

The initial condition of our numerical experiments consists of a concentric bundle of $N = 169$ circular vortex rings placed inside a torus of outer radius $R_0 = 1.2 \times 10^{-2}$ cm and inner radius $a = 3.4 \times 10^{-3}$ cm. These initial rings

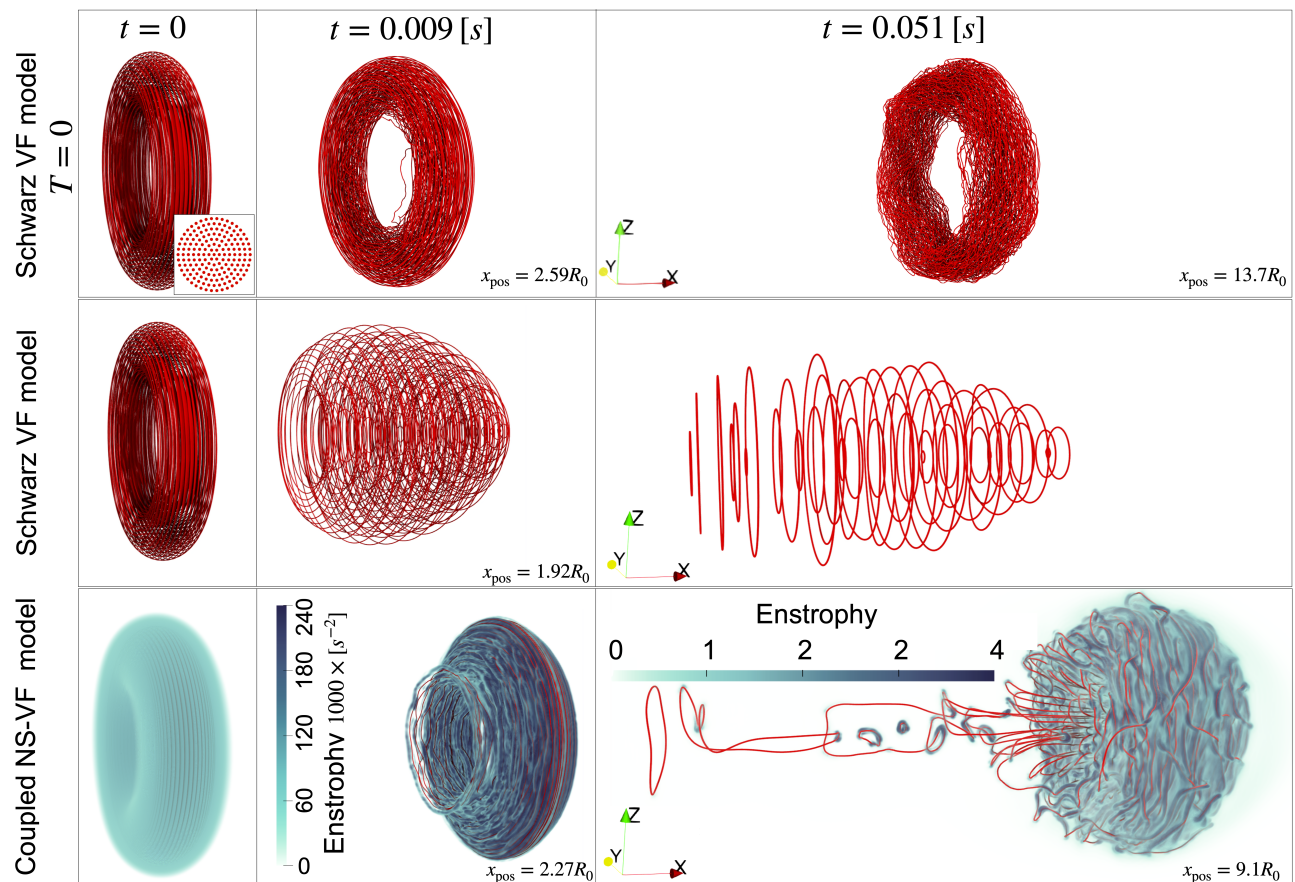


FIG. 1. Evolution of vortex bundle with an initial central radius $R_0 = 1.2 \times 10^{-2}$ cm traveling along the x-direction at $t = 0$, (left column), $t = 0.009$ s (middle column) and $t = 0.051$ s (right column). Vortex lines are displayed in red and the normal fluid's enstrophy in blueish colours. The inset in the top left panel displays the initial cross section of the bundle. Top and middle rows show numerical simulations of Schwarz's VF model at $T = 0$ and $T = 1.95$ K respectively. The distance travelled by the bundle (where it remains coherent) is denoted by x_{pos} . Results obtained using the coupled NS-VF model are shown in the bottom row.

are distributed in a regular hexagonal lattice over the torus cross-section (top left panel of Fig. 1), corresponding to solid-body rotation within the torus. The exact initial vortex configuration does not play a fundamental role, as we obtain the same numerical results with vortices arranged randomly within the toroidal geometry. For comparison, we also study a smaller bundle ($R_0 = 2.3 \times 10^{-2}$ cm, $a = 2.9 \times 10^{-3}$ cm, $R/a = 8$) with only $N = 37$ vortex rings. Although for practical computational reasons we have about 10 times less rings than in experiments, the radius ratio $R_0/a = 3.5$ of the larger bundle is essentially the same as in¹⁷.

III. RESULTS

Firstly we perform simulations at temperature $T = 0$: the normal fluid and the friction are absent (vortices hence move purely according to the Biot-Savart law, Eq. (2)). We find that the vortex bundle preserves its shape for a long time as displayed in Fig. 1 (top). The radii R and a remain almost constant during the computed evolution, while the bundle travels a distance $D \approx 14 R_0$ in the x direction; this is in quantitative agreement with experiments¹⁷ in the low temperature range ($T = 1.3$ K, corresponding to 96 % superfluid fraction). In the initial stage, each vortex rings leapfrogs around and inside the others, until reconnections occur, triggering Kelvin waves, as illustrated in Fig. 1²⁹. Presence of Kelvin waves implies a small increase of the total vortex length $L = \oint_{\mathcal{C}} d\xi$ (green dots in Fig. 2(a)). Only at much later times (not shown), the bundle slowly starts losing coherence.

Secondly, we study the bundle's evolution at $T = 1.95$ K (corresponding to $\rho_n \approx \rho_s$). Using Schwarz's VF model, we observe that, travelling in the normal fluid imposed at rest, the bundle spreads spatially in the direction of motion, rapidly losing its coherence by leaving vortices behind (see Fig. 1 (middle)). The rapid decay of the total vortex

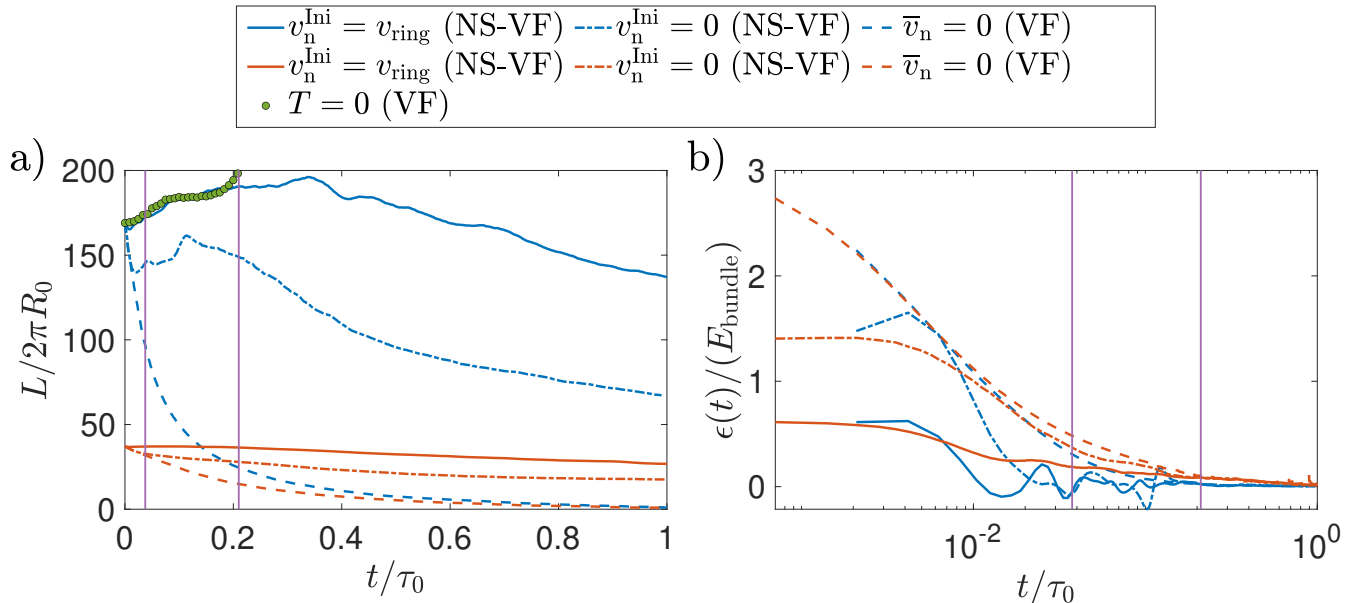


FIG. 2. Temporal evolution of vortex bundle's total length $L(t)$ (a) and energy dissipation $\epsilon(t)$ (b) at $T = 1.95$ K of bundles with $N = 169$ (blue) and $N = 37$ (red) rings. Plots compare Schwarz's VF model (dashed lines) and coupled NS-VF model with (solid lines) and without (dot-dashed lines) an initial normal fluid vortex ring. $T = 0$ temporal evolution is shown by green dots. The two vertical lines correspond to times $t = 0.009$ s and $t = 0.051$ s represented in Fig. 1. The time scale τ_0 is the lifetime of a single quantum vortex ring of initial radius equal to R_0 at $T = 1.95$ K ($\tau_0 = 0.2444$ s and $\tau_0 = 0.9041$ s for the $N = 169$ and the $N = 37$ bundle, respectively).

length is clear in Fig. 2 (a, dashed blue line): by $t = 0.009$ s and $t = 0.051$ s, L has decreased to 60% and 10% of its original value respectively, in stark disagreement with experiments. Essentially, the bundle disassembles into isolated vortex rings which shrink in a time interval comparable to the lifetime $\tau_0 = 0.2444$ s of a single vortex ring of initial radius equal to R_0 at the same temperature $T = 1.95$ K.

We observe a totally different behavior if we use the more realistic coupled NS-VF model²⁴ accounting for the evolving \mathbf{v}_n . As initial condition for \mathbf{v}_n we choose a large-scale toroidal vortex-ring of outer radius R_0 , inner radius a and circulation $N\kappa$ (i.e. matching the superfluid bundle circulation), with a Gaussian distribution of vorticity within the toroidal core (see Fig. 1 (bottom, left)). This is probably a fair approximation to the physical reality of the experiment: as liquid helium is pushed out of the nozzle, a normal fluid vortex ring with the same circulation of the superfluid vortex bundle is indeed observed¹⁷. We find that the vortex bundle does not decay, but remains coherent and travels a significant distance D compared to its diameter ($D \approx 15R_0$), in agreement with experiments¹⁷. The coherence of the coupled normal fluid – superfluid vortex structure can be appreciated in Fig. 1 (bottom), where the normal fluid enstrophy density, $|\omega_n|^2$, is shown (bluish colors) alongside the superfluid quantized vortices (red lines). We observe that the radial distribution of the vorticity is broader compared to the initial condition, also filling the central region of the torus: this is consistent with the experimental report that large-scale helium vortex rings have a less sharp vorticity distribution than vortex rings in classical fluids^{16,17}.

Remarkably, while under Schwarz's VF evolution the total vortex length L rapidly decays, under coupled NS-VF evolution L remains almost constant, see Fig. 2(a), similarly to what happens for $T = 0$. This effect is not simply the consequence of the initially imposed normal fluid ring. We have indeed performed NS-VF simulations with an initially quiescent normal fluid (dot-dashed lines in Fig. 2). We have found that during a short initial stage ($t < 0.02\tau_0$), the coupled NS-VF model follows the rapid decay of the Schwarz's VF model, but after this short transient, the superfluid vortex bundle creates normal fluid vortex structures which prevent the rapid decay of the bundle. The evolution of the smaller vortex bundle ($N = 37$ rings) is similar, as shown by the red curves in Fig. 2. The larger and faster spatial spreading of the initial compact structure as the energy saving mechanism is less efficient, is reminiscent of the behaviour observed in active matter systems³⁰.

A. Dissipation reduction via hydrodynamic cooperation

The normal fluid vortex structures generated by the back-reaction of the superfluid vortex rings are similar to vorticity injection in ordinary viscous fluids by point-like active agents (*e.g.* solid particles in classical turbulence³¹), suggesting that a superfluid can be seen as a peculiar type of active fluid. The mutual friction force per unit length

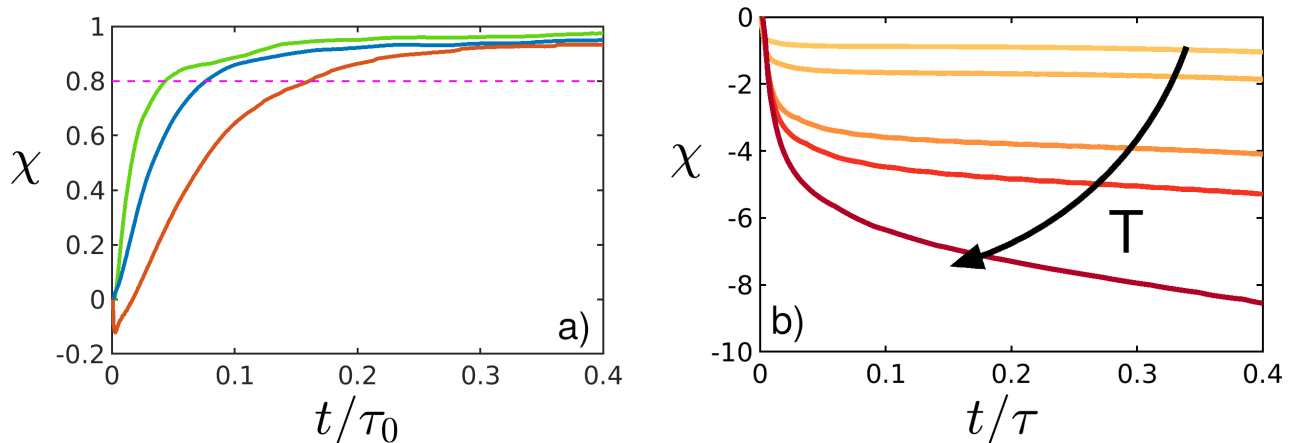


FIG. 3. **a)**: Temporal evolution of dissipation reduction χ for a superfluid vortex bundle with a number of vortices $N = 37$, outer radius $R_0 = 2.3 \times 10^{-2}$ cm and inner radius $a = 2.9 \times 10^{-3}$ cm (green curve, $\ell/\bar{\sigma} = 1.7$), $a = 5.8 \times 10^{-3}$ cm (blue curve, $\ell/\bar{\sigma} = 3.4$) and $a = 1.2 \times 10^{-2}$ cm (red curve, $\ell/\bar{\sigma} = 6.8$). Temperature is $T = 1.95$ K. The horizontal dashed magenta line indicates 80% of dissipation reduction. Time scale τ_0 as in Fig. 2. **b)**: Temporal evolution of χ for an isolated vortex ring of initial radius $R_0 = 7.6 \times 10^{-3}$ cm, moving in an initially quiescent normal fluid at temperatures $T = 1.7, 1.8, 1.95, 2.0, 2.1$ K (from yellow to red); time t is normalized by the vortex ring lifetime τ .

\mathbf{f}_{ns} is a function of the local relative velocity $\dot{\mathbf{s}} - \mathbf{v}_n$ between the vortex line and the local normal fluid velocity. If the coupling between superfluid and normal fluid is sufficiently strong and the intervortex distance is sufficiently small (so that vortices can benefit from the normal fluid stirring performed by other vortices), $|\dot{\mathbf{s}} - \mathbf{v}_n| \rightarrow 0$, reducing the drag and slowing down (even halting) the decay of the combined normal fluid - superfluid vortex structure.

To characterise the dissipation reduction arising from the interaction between vortices and normal fluid, we compute the dissipation of superfluid kinetic energy

$$\epsilon(t) = \oint_{\mathcal{L}} \mathbf{f}_{ns}(\mathbf{s}) \cdot \dot{\mathbf{s}}(\xi, t) d\xi, \quad (5)$$

normalized by $\rho_n \kappa^2 N^2 L(t)$, and report it in Fig. 2(b). Schwarz's VF model (dashed lines) is compared to the coupled NS-VF model with and without an initial normal fluid ring (solid and dot-dashed lines respectively). It is clear that in the coupled model the dissipation is substantially reduced compared to Schwarz's VF model (note that in the VF model, the decrease of friction at large times is related to the small number of distant vortices remaining in the system leading to $\dot{\mathbf{s}} \rightarrow 0$).

Two concurring mechanisms are likely to be responsible for this observed reduced dissipation in the coupled model: the coupling itself, which reduces the velocity difference $\dot{\mathbf{s}} - \mathbf{v}_n$ between a *single* vortex ring and the normal fluid, and the collective hydrodynamic cooperation, where vortices benefit from the normal fluid stirring performed by other vortices. To determine the relevance of collective effects, we study the impact of the average intervortex distance on the dissipation reduction, by numerically simulating the dynamics of bundles with different initial inner radii a and computing the dissipation reduction χ with respect to the initial condition, defined as $\chi(t) = (\epsilon(0) - \epsilon(t))/(\epsilon(0))$. The initial condition of the normal fluid is quiescent, as this allows to better appreciate the stirring of the normal fluid performed by superfluid vortices and the consequent dissipation reduction. The temporal evolution of χ is illustrated in Fig. 3(a) where it clearly emerges that the dissipation reduction is more efficient when a is smaller. The time interval which the system requires to reduce the initial dissipation $\epsilon(0)$ by 80% (magenta dashed line in Fig. 3(a)), is almost proportional to a . This observed less efficient dissipation reduction as a increases is determined by the following factors: the stirring of the normal fluid is weaker, given that the vortex velocity is smaller ($\dot{\mathbf{s}} \sim 1/a$), and the hydrodynamic interactions are less intense as vortices are further apart. This last feature is characteristic of active fluid systems, as observed for drafting particles in optical vortices⁷, for cyclists facing a steep hill where drafting is negligible³⁰ and in the role played by ejection delay in the dispersion of fungal spores⁴.

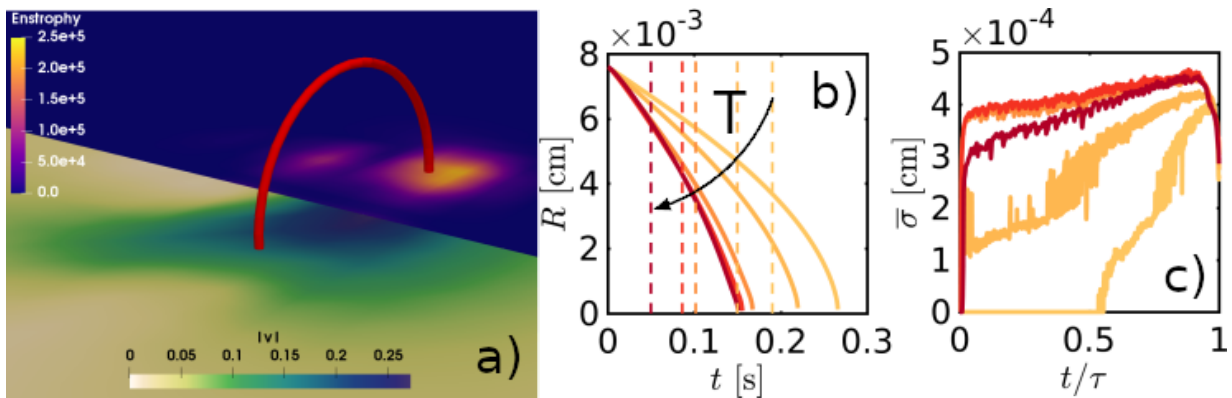


FIG. 4. Coupled NS-VF model. Normal fluid flow disturbances at $T = 1.95$ K generated by a single superfluid vortex ring of initial radius $R_0 = 7.6 \times 10^{-3}$ cm traveling from left to right. **a)** normal fluid's enstrophy $|\omega_n|^2$ (in s^{-2} , top) and speed $|\mathbf{v}_n|$ (in cm/s, bottom) plotted on the horizontal plane $z = 0$ at time $t = 0.16$ s; the superfluid vortex ring is the red tube. **b)** Temporal evolution of the radius R (in cm) of an isolated vortex ring of initial radius $R_0 = 7.6 \times 10^{-3}$ cm, moving in an initially quiescent normal fluid at temperatures $T = 1.7, 1.8, 1.95, 2.0, 2.1$ K (from yellow to red) **c)** Temporal evolution of the size $\bar{\sigma}$ of the normal fluid flow disturbances generated by the shrinking vortex ring; colors as in b); time t is normalized by the vortex ring lifetime τ .

To assess the role played by the coupling on its own, we study, employing the coupled NS-VF model, the dynamics of a single, isolated vortex ring of initial radius $R_0 = 7.6 \times 10^{-3}$ cm, in an initially quiescent normal fluid. Panel a) of Fig. 4 shows the isolated superfluid vortex ring (in red) traveling from left to right at $t = 0.16$ s when the temperature $T = 1.95$ K. The normal fluid enstrophy density $|\omega_n|^2$ and the magnitude of the normal fluid velocity, $|\mathbf{v}_n|$, are displayed respectively in the upper and lower halves of the horizontal plane $z = 0$ (perpendicular to the plane containing the superfluid vortex ring). We observe two enstrophy structures which can be thought as two vortex rings in the normal fluid²⁵. Similar normal fluid enstrophy structures are also visible near all vortex lines in a bundle, see Fig. 1 (bottom row).

As the isolated superfluid vortex ring moves in the normal fluid and perturbs it, it loses energy: its radius R therefore shrinks with time, as shown in Fig. 4(b), with corresponding lifetimes τ decreasing for increasing temperatures³². Lifetimes of vortex rings predicted by the coupled NS-VF model are roughly twice the lifetimes predicted by Schwarz's VF model (indicated by vertical dashed lines in Fig. 4(b)): the inclusion of the coupling in the model indeed reduces the dissipation with respect to Schwarz's VF model. However, if we compute the dissipation reduction $\chi(t)$ during the shrinking of the rings (Fig. 3(b)), we observe that the dissipation actually increases with respect to its initial value ($\chi < 0$). Hence, the dissipation reduction ($\chi \rightarrow 1$) observed in the dynamics of bundles, responsible for their significantly enhanced lifetime (larger than τ_0 , see Fig. 2(a)), consistent with experimental measurements, uniquely stems from collective hydrodynamic cooperation.

By employing an enstrophy-weighted average approach (see Appendix A), we calculate the typical size $\bar{\sigma}$ of the normal fluid enstrophy structures generated by vortex rings and report its temporal behaviour in Fig. 4(c). Subsequently we compute the dimensionless ratio $\ell/\bar{\sigma}$, $\ell = a\sqrt{\pi/N}$ being the initial average intervortex spacing, obtaining $0.93 \lesssim \ell/\bar{\sigma} \lesssim 1.7$ (simulations in Fig. 2) and $1.7 \lesssim \ell/\bar{\sigma} \lesssim 6.8$ (simulations in Fig. 3(a)): this range of values assumed by $\ell/\bar{\sigma}$ implies that the normal fluid perturbations indeed play a role in the vortex bundle dynamics, confirming the hydrodynamic cooperative nature of the dissipation reduction observed. Interestingly, the values of $\bar{\sigma}$ are comparable to the size of solid hydrogen tracking particles used in current experiments, reinforcing recent suggestions ascribing the observed statistics of particle velocities also to the indirect interaction between particle and vortices, *i.e.* via the disturbances generated in the normal fluid by superfluid vortices^{23,33}.

IV. CONCLUSIONS

Using our coupled NS-VF model which takes in full account²⁴ the reciprocal interaction of the superfluid and the normal fluid, we have found that a compact bundle of superfluid vortex rings creates a disturbance in the normal fluid that is sufficiently strong to reduce the overall velocity difference between the two fluids, hence reduce the friction on the superfluid vortex rings. While isolated superfluid vortex rings quickly lose energy, shrink and vanish, we observe that bundled vortex rings remain coherent and travel a significant distance compared to their size, as observed in the experiments¹⁵⁻¹⁷. We have also found that the bundle remains coherent in the limit of zero temperature (no normal

fluid), again in agreement with experiments and previous works²⁹.

We show that the observed dissipation reduction in bundles is a collective effect stemming from the hydrodynamic cooperation of vortices. This cooperation is similar to what has been observed in systems of active particles such as swimming bacteria¹⁻³, fungal spores⁴, racing cyclists^{5,6} and particle pairs trapped in an optical vortex^{7,8}, in which self-organized structures emerge from energy-saving mechanisms³⁰. The system that we have investigated, superfluid helium, is however richer: whereas in fact in the cited active matter systems the agents, besides modifying the common background fluid, may interact with each others directly only via short-range two-body collisions, in our case vortex lines also experience a significant collective long-range Biot-Savart interaction which, for instance, induces them to collectively rotate around each other (leapfrogging). Superfluid helium can hence be considered as a peculiar kind of active fluid, distinguished by a 4-way coupled dynamics which potentially determines characteristics of turbulence in both superfluid and normal fluid components.

The effect of coupling and drag reduction on the statistics of superfluid turbulence and on other integral quantities (such as helicity³⁴ if for instance the initial bundle is twisted) will be the topic of future research, as well as the implications for vortex dynamics in the more viscous helium isotope ³He.

ACKNOWLEDGMENTS

Acknowledgments. We are grateful to the Royal Society for supporting this project (award n. IES \R2\181176). LG and CFB acknowledge the support of the Engineering and Physical Sciences Research Council (Grant No. EP/R005192/1). LG acknowledges the support of Istituto Nazionale di Alta Matematica (INdAM). GK was supported by the Agence Nationale de la Recherche (project GIANT ANR-18-CE30-0020-01). Computations were carried out at the Mesocentre SIGAMM, hosted at the Observatoire de la Cote d'Azur, and at the HPC Rocket Cluster at Newcastle University.

Appendix A: Calculation of $\bar{\sigma}(t)$

The centre $\mathbf{x}_\omega(t)$ of the normal fluid enstrophy distribution $|\boldsymbol{\omega}_n(\mathbf{x}, t)|^2$ on the $z = 0$ plane is calculated as follows,

$$\mathbf{x}_\omega(t) = \frac{\iint \mathbf{x} |\boldsymbol{\omega}_n(\mathbf{x}, t)|^2 d\mathbf{x}}{\iint |\boldsymbol{\omega}_n(\mathbf{x}, t)|^2 d\mathbf{x}}, \quad (\text{A1})$$

where $\mathbf{x}_\omega(t) = (x_\omega(t), y_\omega(t), 0)$ and $\mathbf{x} = (x, y, 0)$ as the calculation is performed on the $z = 0$ plane.

The normal fluid vortex size $\bar{\sigma}$ whose temporal evolution is reported in Fig. 4 (b) is given by $\bar{\sigma}(t) = \sqrt{R_n(t) R_t(t)}$ where R_n and R_t are computed as follows,

$$R_n^2(t) = \frac{\iint [(\mathbf{x} - \mathbf{x}_\omega(t)) \cdot \hat{\mathbf{n}}(t)]^2 |\boldsymbol{\omega}_n(\mathbf{x}, t)|^2 d\mathbf{x}}{\iint |\boldsymbol{\omega}_n(\mathbf{x}, t)|^2 d\mathbf{x}}, \quad (\text{A2})$$

$$R_t^2(t) = \frac{\iint [(\mathbf{x} - \mathbf{x}_\omega(t)) \cdot \hat{\mathbf{t}}(t)]^2 |\boldsymbol{\omega}_n(\mathbf{x}, t)|^2 d\mathbf{x}}{\iint |\boldsymbol{\omega}_n(\mathbf{x}, t)|^2 d\mathbf{x}}, \quad (\text{A3})$$

where $\hat{\mathbf{t}}(t)$ is the unit vector indicating the direction of the mutual friction force $\mathbf{f}_{ns}(t)$ exerted by the vortex ring onto the normal fluid on the $z = 0$ plane, and $\hat{\mathbf{n}}(t)$ is the orthogonal direction to $\hat{\mathbf{t}}(t)$ lying on $z = 0$ plane.

Appendix B: The NS-VF model

The numerical methods used to implement Schwarz's VF and the coupled NS-VF models are described in detail in Ref.²⁴. Here we summarize the main characteristics of the coupled NS-VF model.

1. Superfluid vortex tangle and normal fluid velocity field evolution

The temporal evolution of the superfluid vortex tangle \mathcal{L} is performed employing the well-established Lagrangian VF method elaborated by Schwarz^{18,35} which discretizes vortex lines in a finite number of line elements whose equation of motion is given by Eq. (1) in the main manuscript. The singularity of the Biot-Savart integral, Eq. (2) in the main manuscript, is regularized by taking into account the finite size of the vortex core¹⁸. We compute the full Biot-Savart integral (no tree-approximation). As reconnections are not intrinsically predicted by the VF method, an additional algorithm has to be employed changing the topology of the vortex configuration when two vortex lines become closer than a set threshold.

The evolution of the normal fluid velocity field \mathbf{v}_n is computed integrating the Navier-Stokes equations (Eqs. (3) - (4) in main manuscript) using a standard pseudo-spectral code de-aliased employing the 2/3-rule. We refer to established literature for further details concerning the standard algorithm employed for the numerical integration of the Navier Stokes equations³⁶.

2. Mutual friction force

The distinguishing features of our coupled NS-VF algorithm actually concern the modeling of the mutual friction force per unit length \mathbf{f}_{ns} in Eq. (4) of the main manuscript. We describe the interaction between superfluid vortices and the normal fluid employing a classical low Reynolds number approach³⁷ revisiting a recent framework used in superfluid turbulence²⁷. According to this approach, the mutual friction force which the superfluid vortices exert on the normal fluid reads as follows,

$$\mathbf{f}_{ns}[\mathbf{s}] = -D \mathbf{s}' \times [\mathbf{s}' \times (\dot{\mathbf{s}} - \mathbf{v}_n)] - \rho_n \kappa \mathbf{s}' \times (\dot{\mathbf{s}} - \mathbf{v}_n) \quad , \quad (\text{B1})$$

where the drag coefficient $D = D[\mathbf{s}]$ is

$$D = \frac{4\pi\rho_n\nu_n}{\left[\frac{1}{2} - \gamma - \ln\left(\frac{|\mathbf{v}_{n\perp} - \dot{\mathbf{s}}|a_0}{4\nu_n}\right)\right]} \quad , \quad (\text{B2})$$

$\gamma = 0.5772$ being the Euler-Mascheroni constant, \mathbf{v}_n is evaluated on the vortex lines, that is to say $\mathbf{v}_n = \mathbf{v}_n[\mathbf{s}]$ (the interpolation being performed using fourth-order *B-splines*), and the quantity $\mathbf{v}_{n\perp}$ indicates the component of the normal fluid velocity lying on a plane orthogonal to \mathbf{s}' . The use of the expression (B1) for \mathbf{f}_{ns} leads to a recalculation of friction coefficients α and α' in Eq. (1) of the main manuscript, as reported in the next section.

As the mutual friction force \mathbf{f}_{ns} is δ -supported on the vortex lines, its numerical distribution on the Eulerian computational grid where we compute the normal fluid velocity \mathbf{v}_n must be handled with care, in order to avoid spurious numerical artifacts. To address this issue, we adopt the same rigorous regularization approach which has been used to take into account the strongly localized response of active point-like particles in classical turbulence³¹. The advantage of adopting this method is that the regularization of the exchange of momentum between point-like active agents and viscous flows is based on the physics of the generation of vorticity and its viscous diffusion at very small scales. In our case, the justification for the use of this model arises from the very small Reynolds numbers characterizing the normal fluid disturbances generated by the moving superfluid vortices ($\text{Re} \approx 10^{-5} \div 10^{-4}$).

3. Calculation of friction coefficients in the coupled NS-VF model

Here we briefly describe the derivation of the expression of the mutual friction coefficients in the coupled NS-VF model (for further details, the reader is referred to Ref.²⁴). The starting point is the classical, low Reynolds number theoretical approach which we employ to model the mutual friction force. This framework leads to Eq. (4) in the main manuscript accounting for the force per unit length $-\mathbf{f}_{ns}$ which the normal fluid exerts onto the superfluid vortices. The superfluid vortices also suffer a Magnus force \mathbf{f}_M as they are immersed in an inviscid fluid (the superfluid) surrounded by a circulation and in relative motion with respect to the superfluid itself. The expression of the Magnus force per unit length exerted onto the superfluid vortices is as follows,

$$\mathbf{f}_M = \rho_s \kappa \mathbf{s}' \times (\dot{\mathbf{s}} - \mathbf{v}_s) \quad . \quad (\text{B3})$$

Since the vortex core is much smaller than any other scales of the flow, the vortex inertia can be neglected and as a consequence the sum of all forces acting on the vortices vanishes, *i.e.* $\mathbf{f}_M - \mathbf{f}_{ns} = 0$. Assuming that each vortex

line element moves orthogonally to its unit tangent vector, *i.e.* $\dot{\mathbf{s}} \cdot \mathbf{s}' = 0$, the balance of forces leads to the following equation of motion,

$$\dot{\mathbf{s}} = \mathbf{v}_{s_\perp} + \beta \mathbf{s}' \times (\mathbf{v}_n - \mathbf{v}_s) + \beta' \mathbf{s}' \times [\mathbf{s}' \times (\mathbf{v}_n - \mathbf{v}_s)] , \quad (\text{B4})$$

where \mathbf{v}_{s_\perp} indicates the component of the superfluid velocity lying on a plane orthogonal to \mathbf{s}' and β and β' are the redetermined mutual friction coefficients for the coupled model.

The expressions for β and β' are as follows,

$$\beta = \frac{a}{(1+b)^2 + a^2} > 0, \quad \beta' = -\frac{b(1+b) + a^2}{(1+b)^2 + a^2} < 0$$

where

$$a = \frac{D}{\rho_s \kappa} = 4\pi \left(\frac{\rho_n}{\rho_s} \right) \left(\frac{\nu_n}{\kappa} \right) \frac{1}{[\frac{1}{2} - \gamma - \ln \left(\frac{|\mathbf{v}_{n_\perp} - \dot{\mathbf{s}}| a_0}{4\nu_n} \right)]}$$

and $b = \frac{\rho_n}{\rho_s}$. Thus, from the physical point of view, the motion of the vortices is governed only by temperature and pressure, determining ρ_n/ρ_s and ν_n/κ , and the normal fluid Reynolds number $\text{Re} = |\mathbf{v}_{n_\perp} - \dot{\mathbf{s}}| a_0 / \nu_n$. In the numerical simulations, we employ values of the densities ρ_n and ρ_s and of the normal fluid kinematic viscosity ν_n consistent with temperature $T = 1.95\text{K}$ at saturated vapor pressure³⁸. Correspondingly, also the values of the friction coefficients α and α' employed in the Schwarz VF model are consistent with experimental values³⁸.

Appendix C: Physical and numerical parameters

1. Superfluid vortex tangle simulations

Following the VF model elaborated by Schwarz^{18,35}, we discretize the vortex tangle \mathcal{L} in a set of N_p vortex line elements centered in $\mathbf{s}_i(t) = \mathbf{s}(\xi_i, t)$, $i = 1, \dots, N_p$, where $\xi_i = i\Delta\xi$ is the discretized arclength with discretization $\Delta\xi \in [\delta, 2\delta]$ where $\delta = 4.0 \times 10^{-4}\text{cm}$. The normal fluid is solved on a three-dimensional computational grid with $\{N_x, N_y, N_z\} = \{512, 512, 512\}$ collocation points in each cartesian direction. The computational domain is a periodic box of size $L_x \times L_y \times L_z$ with $L_x = L_y = L_z = 10^{-1}\text{cm}$ which leads to grid spacings $\Delta x = \Delta y = \Delta z = 1.95 \times 10^{-4}\text{cm}$. The size of the computational box is identical for the calculation of the vortex filaments ($L_x = L_y = L_z = 10^{-1}\text{cm}$) and also in this calculation we use periodic boundary conditions. The time step Δt employed in the computation of the temporal evolution of the ‘large’ bundle ($N = 169$, cf. main manuscript) is $\Delta t = 5.0 \times 10^{-6}\text{s}$, while the time step used for the ‘thin’ bundle ($N = 37$) is $\Delta t = 6.25 \times 10^{-6}\text{s}$. In order to distribute the mutual friction force \mathbf{F}_{ns} over the computational grid where the normal fluid velocity is resolved, before employing the regularization adopted in classical turbulence³¹, we interpolate the vortex filaments with a cubic kernel over an arc-length sub-scale $\Delta\xi/4$. We validated this interpolation method on the motion of individual vortex rings.

2. Single superfluid vortex ring simulations

In this set of simulations whose results are summarized in Fig. 3(b) and 4, we use a finer discretization of the vortex lines, δ being equal to $8.0 \times 10^{-5}\text{cm}$. This results in a smaller time step $\Delta t_{\text{VF}} = 6.25 \times 10^{-7}\text{s}$. For the normal fluid velocity computation we use $\{N_x, N_y, N_z\} = \{256, 256, 256\}$ collocation points in each cartesian direction leading to $\Delta x = \Delta y = \Delta z = 3.90 \times 10^{-4}\text{cm}$, as the computational periodic box is $L_x \times L_y \times L_z$ with $L_x = L_y = L_z = 10^{-1}\text{cm}$. The time step employed for the calculation of the normal fluid velocity field is $\Delta t_{\text{NS}} = 2.50 \times 10^{-5}\text{s}$.

¹ López H, Gachelin J, Douarche C, Auradou H, Clément E (2015) Turning bacteria suspensions into superfluids. *Phys. Rev. Lett.* 115:028301.

² Martinez VA, et al. (2020) A combined rheometry and imaging study of viscosity reduction in bacterial suspensions. *Proc. Nat. Acad. Sci. USA* 117(5):2326–2331.

³ Guo S, Samanta D, Peng Y, Xu X, Cheng X (2018) Symmetric shear banding and swarming vortices in bacterial superfluids. *Proc. Nat. Acad. Sci. USA* 115(28):7212–7217.

- ⁴ Roper M, et al. (2010) Dispersal of fungal spores on a cooperatively generated wind. *Proc. Nat. Acad. Sci. USA* 107:17474.
- ⁵ Blocken B, et al. (2018) Aerodynamic drag in cycling pelotons: New insights by cfd simulation and wind tunnel testing. *J. Wind Eng. Ind. Aeronautics* 179:319.
- ⁶ Belden J, et al. (2019) How vision governs the collective behaviour of dense cycling pelotons. *J. R. Soc. Interface* 16:20190197.
- ⁷ Reichert M, Stark H (2004) Circling particles and drafting in optical vortices. *J. Phys. Condens. Matt.* 16:S4085.
- ⁸ Grujic K, Helleso O (2007) Dielectric microsphere manipulation and chain assembly by counter-propagating waves in a channel waveguide. *Opt. Express* 15:10.
- ⁹ Gamota G (1973) Creation of quantized vortex rings in superfluid helium. *Phys. Rev. Lett.* 31:517.
- ¹⁰ Walmsley P, Golov A (2008) Quantum and quasiclassical types of superfluid turbulence. *Phys. Rev. Lett.* 100:245301.
- ¹¹ Walmsley P, Golov A (2014) Reconnections of quantized vortex rings in superfluid ⁴he at very low temperatures. *Phys. Rev. Lett.* 113:125302.
- ¹² Guenin B, Hess G (1978) Observations of quantized vorticity generated in superfluid ⁴he flow through 2 – μ m-diameter orifices. *J. Low Temp. Phys.* 33:243.
- ¹³ Bradley D, et al. (2005) Emission of discrete vortex rings by a vibrating grid in superfluid ³he-b: a precursor to quantum turbulence. *Phys. Rev. Lett.* 95:035302.
- ¹⁴ Barenghi CF, Donnelly RJ (2009) Vortex rings in classical and quantum systems. *Fluid Dyn. Res.* 41:051401.
- ¹⁵ Borner H, Schmeling T, Schmidt D (1981) Experimental investigation of the circulation of large scale vortex rings in he ii. *Physica B* 108:1123.
- ¹⁶ Borner H, Schmeling T, Schmidt D (1983) Experiments on the circulation and propagation of large scale vortex rings in he ii. *Phys. Fluids* 26:1410.
- ¹⁷ Borner H, Schmidt D (1985) Investigation of large-scale vortex rings in he ii by acoustic measurements of circulation. *Lecture Notes in Physics* 235:135.
- ¹⁸ Schwarz K (1988) Three-dimensional vortex dynamics in superfluid ⁴he: homogeneous superfluid turbulence. *Phys. Rev. B* 38:2398.
- ¹⁹ Araki T, Tsubota M, Nemirovskii S (2002) Energy spectrum of superfluid turbulence with no normal-fluid component. *Phys. Rev. Lett.* 89:145301.
- ²⁰ Baggaley AW, Laurie J, Barenghi CF (2012) Vortex-density fluctuations, energy spectra, and vortical regions in superfluid turbulence. *Phys. Rev. Lett.* 109:205304.
- ²¹ Donnelly RJ, Barenghi CF (1998) The observed properties of liquid helium at the saturated vapor pressure. *J. Phys. Chem. Ref. Data* 27:1217.
- ²² Guo W, Cahn SB, Nikkel JA, Vinen WF, McKinsey DN (2010) Visualization study of counterflow in superfluid helium-4 using metastable helium molecules. *Phys. Rev. Lett.* 105:045301.
- ²³ Mastracci B, Bao S, Guo W, Vinen WF (2019) Particle tracking velocimetry applied to thermal counterflow in superfluid he 4: Motion of the normal fluid at small heat fluxes. *Phys. Rev. Fluids* 4(8):083305.
- ²⁴ Galantucci L, Baggaley AW, Barenghi CF, Krstulovic G (2020) A new self-consistent approach of quantum turbulence in superfluid helium. *Eur. Phys. J. Plus* 135:547.
- ²⁵ Kivotides D, Barenghi CF, Samuels DC (2000) Triple vortex ring structure in superfluid helium ii. *Science* 290:777.
- ²⁶ Galantucci L, Sciacca M, Barenghi CF (2015) Coupled normal fluid and superfluid profiles of turbulent helium ii in channels. *Phys. Rev. B* 92:174530.
- ²⁷ Kivotides D (2018) Superfluid helium-4 hydrodynamics with discrete topological defects. *Phys. Rev. F* 3:104701.
- ²⁸ Yui S, Kobayashi H, Tsubota M, Guo W (2020) Fully coupled dynamics of the two fluids in superfluid ⁴ he: Anomalous anisotropic velocity fluctuations in counterflow. *Phys. Rev. Lett.* 124:155301.
- ²⁹ Wacks DH, Baggaley AW, Barenghi CF (2014) Coherent laminar and turbulent motion of toroidal vortex bundles. *Phys. Fluids* 26:027102.
- ³⁰ Trenchard H, Perc M (2016) Energy saving mechanisms, collective behavior and the variation range hypothesis in biological systems: A review. *Biosystems* 147:40.
- ³¹ Gualtieri P, Picano F, Sardina G, Casciola C (2015) Exact regularized point particle method for multiphase flows in the two-way coupling regime. *J. Fluid Mech.* 773:520–561.
- ³² Barenghi CF, Donnelly RJ, Vinen WF (1983) Friction on quantized vortices in helium ii. a review. *J. Low Temp. Phys.* 52(3/4):189.
- ³³ Svancara P, Duda D, Hrubcová P, Rotter M, Skrbek L, La Mantia M, Durozoy E, Diribarne P, Rousset B, Bourgoin M and M. Gibert (2021) Ubiquity of particle-vortex interactions in turbulent counterflow of superfluid helium *J Fluid Mech* 911:A8.
- ³⁴ Galantucci L, Barenghi CF, Parker NG, Baggaley, AW (2021) Mesoscale helicity distinguishes Vinen from Kolmogorov turbulence in helium-II. *Phys. Rev. B* 013:144503.
- ³⁵ Hänninen R, Baggaley AW (2014) Vortex filament method as a tool for computational visualization of quantum turbulence. *Proc. Nat. Acad. Sci. USA* 111:4667-4674 suppl. 1.
- ³⁶ Gottlieb D, Orszag S (1977) *Numerical analysis of spectral methods: theory and applications.* (SIAM).
- ³⁷ Proudman I, Pearson J (1957) Expansions at small Reynolds numbers for the flow past a sphere and a circular cylinder. *J. Fluid Mech.* 2:237.
- ³⁸ Donnelly R, Barenghi C F (1998) The observed properties of liquid helium at saturated vapor pressure. *J. Phys. Chem. Ref. Data* 27:1217.